ChemComm

COMMUNICATION

View Article Online
View Journal | View Issue



Cite this: *Chem. Commun.*, 2025, **61**, 3852

Received 9th December 2024,
Accepted 31st January 2025

DOI: 10.1039/d4cc06478j

rsc.li/chemcomm



# A single-crystal 3D Zn-tetrathiolate connected metal–organic framework†

Jian-Rong Li,‡[a] Jieying Hu,‡[a] Long Jiang,[c] Yonghe He,[a] Wei-Ming Liao,[ab] Xianghua Yang,[a] Lai-Hon Chung *[ab] and Jun He *[ab]

**Due to thiolate's fast and robust coordination, crystallographically resolved thiolate-ligated metal–organic frameworks (MOFs) are hard to obtain. Following the previous success of the masked synthetic strategy to achieve single-crystal Pb-thiolate connected MOFs, thioester-protected hexathiotriphenylene (HVaTT) was employed in this work to assemble with a Zn(II) centre to yield the first example of a first-row transition-metal based crystallographically resolved metal-tetrathiolate connected MOF, HTT-Zn. HTT-Zn features a 3D anionic framework connected by tetrahedral [$ZnS_4$] nodes with 3-fold interpenetration and windmill-like topology. Thanks to the anionic nature, HTT-Zn demonstrates a fast colorimetric response (from yellow to black) to the positively charged toxic pollutant, paraquat, and potentially serves as a naked-eye sensor for paraquat. Isolation of HTT-Zn proves masked synthesis as a general approach and adds a new dimension to explore metal-thiolate-based MOFs.**

Thiol metal–organic frameworks (S-MOFs), a subcategory of MOFs, are composed of thiol-containing organic linkers and metal nodes. Owing to the redox activeness and intense interaction with heavy/transition metal centres of electronically diffused thiolate, S-MOFs usually feature rich activity, decent conductivity, *etc.* These properties allow S-MOFs to excel in a wide range of applications including conductivity,[1] photocatalysis,[2] electrocatalysis,[3] energy storage,[4] sensing,[5] heavy metal adsorption,[6] *etc.*

Generally, there are two types of S-MOF: (1) frameworks composed of metal ions and linkers bearing carboxyl and thiol groups (aka Mercarb linker);[7] (2) planar π-conjugated two-dimensional (2D) networks built from soft metal ions and linkers equipped with three dithiolate ends (*e.g.* 2,3,6,7,10,11-hexakis(thiolate)triphenylene, $HTT^{6-}$).[8] Carboxyl groups in the Mercarb linker withdraw the electron density of thiol and slow down the formation of the M–S bond on the one hand, while they coordinate the metal centre reversibly on the other hand to facilitate assembly of crystalline S-MOF, suitable for resolving single-crystal structure.[9] However, strongly coordinating $HTT^{6-}$ chelate metal centres so fast that the S-MOFs obtained are usually poor in crystallinity, let alone single-crystal structure determination. This type of S-MOF typically adopts a 2D planar network connected by metal-bis(dithiolene) nodes and is prepared by solvothermal or biphasic interfacial diffusion methods.[10] To expose the metal-bis(dithiolene) active sites and explore structure–property correlation, obtaining three-dimensional (3D) crystallographically resolved thiolate-ligated S-MOFs is insightful. Yet, limited by the fast and strong coordination of thiolate, only two single-crystal 3D analogues of this type of S-MOF have been reported by our group.[11]

To slow down the coordination for the framework of higher crystallinity and even obtain crystals suitable for single-crystal determination, we proposed a masked strategy to functionalise thiol as thioester, which is not just bench-stable (as thiol is more susceptible to oxidation under air) but can be easily deprotected during assembly for an extended coordination process. Specifically, thiol-masked linker, 2,3,6,7,10,11-hexakis(pentanoylthio)triphenylene (HVaTT), was prepared and allowed to assemble with Pb(II) salt in basic medium (for deprotection) to give two examples of single-crystal Pb-based S-MOFs.[11] Utilising the same strategy, we successfully extend the scope to first-row transition metals and herein report a crystallographically resolved 3-fold interpenetrated Zn-based S-MOF.

HVaTT (Fig. S1 and S2 (ESI†)), prepared from a modified procedure of our work,[11b] was allowed to react solvothermally with $Zn(OAc)_2{\cdot}2H_2O$ in methanol (MeOH) in the presence of ethylenediamine (EDA, as modulator to temporarily occupy Zn(II) ions) and NaOH (for *in situ* hydrolysis of HVaTT to $HTT^{6-}$) at 120 °C for 48 h to obtain **HTT-Zn** as yellow block-shaped

[a] *School of Chemical Engineering and Light Industry, Guangdong University of Technology, Guangzhou 510006, P. R. China. E-mail: junhe@gdut.edu.cn, laihonchung@gdut.edu.cn*
[b] *Guangdong Provincial Laboratory of Chemistry and Fine Chemical Engineering Jieyang Center, Jieyang 515200, China*
[c] *MOE Key Laboratory of Bioinorganic and Synthetic Chemistry, School of Chemistry and Chemical Engineering, Sun Yat-Sen University, Guangzhou 510275, China*

† Electronic supplementary information (ESI) available: Preparation details of HVaTT and **HTT-Zn**, spectroscopic data, and additional plots/figures. Contains the supplementary crystallographic data for **HTT-Zn**. CCDC 2407349. For ESI and crystallographic data in CIF or other electronic format see DOI: https://doi.org/10.1039/d4cc06478j

‡ These authors contributed equally.

crystals (Fig. 2b and Fig. S3, ESI†). Noteworthily, unprotected HTT could only give **HTT-Zn** of far worse crystallinity upon assembly with Zn(II) ions, highlighting the masked strategy as an effective tactic to obtain highly crystalline S-MOFs.

A block-shaped **HTT-Zn** single crystal was analysed by single-crystal X-ray diffraction (SCXRD). The crystal data indicate that **HTT-Zn** adopts a hexagonal crystal system with a space group of $P6_3/m$ and lattice parameters of $a = b = 30.4115$ Å, $c = 56.222$ Å, $\alpha = \beta = 90^\circ$, $\gamma = 120^\circ$. Each Zn(II) centre is chelated by two sets of dithiolate (Fig. 1a, note: Zn–S bond ~2.36 Å, comparable to single Zn–S bond reported in other molecular systems[12]) from two $HTT^{6-}$ linkers to give a tetrahedral four-coordinated [$ZnS_4$] unit (Fig. 1b) rather than the well-known planar metal-bis(dithiolene), [$MS_4$], site as a secondary building unit (SBU). Each triangular $HTT^{6-}$ is trigonally connected to three SBUs, forming an infinitely expanding 3D structure. Viewed along the *c*-axis (Fig. 1c), taking $HTT^{6-}$ and $Zn^{2+}$ as a triangle and stick, the framework can be simplified to a windmill-like topology. The windmill-like 3D network can be described as a new 2,2,2,3,3,3-*c* net calculated by ToposPro software. The dihedral angle between adjacent $HTT^{6-}$ planes surrounding the windmill disc is about 85° whereas that between adjacent $HTT^{6-}$ planes forming the windmill blades is about 90°. Note that **HTT-Zn** exhibits 3-fold interpenetration where the disc of one windmill alternately intertwines with the blades of two other windmills (Fig. 1d and e). **HTT-Zn** features an anionic framework bearing a formula unit of $[Zn_3(C_{18}H_6S_6)_2]^{6-}$, with the negative charge being balanced by the $Na^+$ ions in the channel. The existence of EDA was also verified by $^1H$ NMR spectroscopy (Fig. S4, ESI†). Scanning electronic microscopy (SEM) reveals

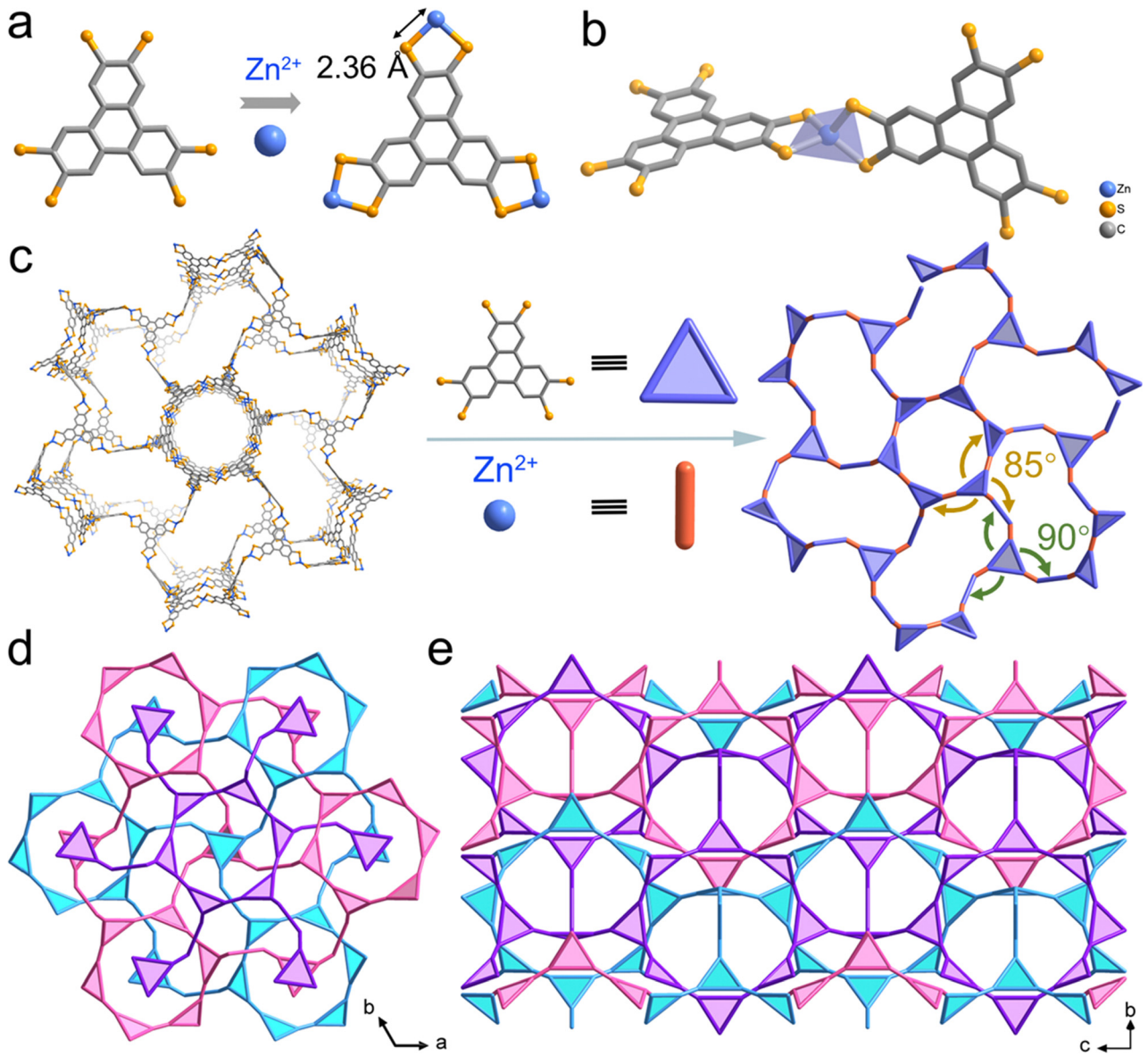


Fig. 1 (a) Self-assembly of $HTT^{6-}$ and Zn(II) ions; (b) coordination environment of the Zn(II) centre; (c) 3D framework and topological network of **HTT-Zn**; representation of the 3-fold interpenetration network of **HTT-Zn** along the (d) *c*-axis and (e) *a*-axis directions.

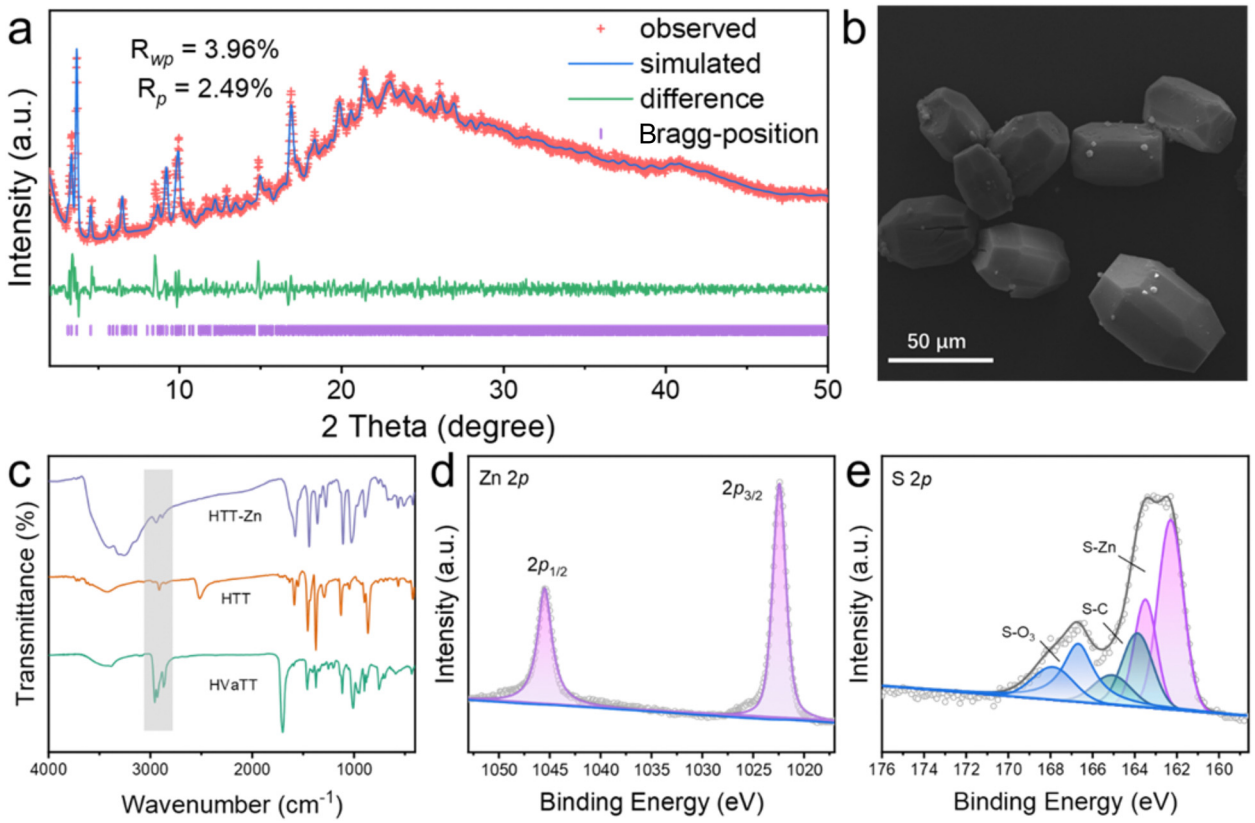


Fig. 2 (a) Rietveld refinement of the experimental PXRD pattern of **HTT-Zn** ($R_{wp}$ = 3.96%; $R_p$ = 2.49%). (b) SEM images of **HTT-Zn**. (c) FT-IR spectra of HVaTT, HTT and **HTT-Zn**. High-resolution XPS spectra of (d) Zn 2p, and (e) S 2p of **HTT-Zn**.

the **HTT-Zn** blocks to be elongated hexagonal-based polyhedra. Energy dispersive X-ray spectroscopy (EDS) analysis indicates the presence and uniform distribution of C, N, S, Zn and Na (Fig. S5, ESI†). Together with the elemental analysis (EA) data, the formula of **HTT-Zn** could be fitted as $Zn_3(C_{18}H_6S_6)_2(Na)_6(C_2H_8N_2)_{3.6}(H_2O)_9$. The satisfactory Rietveld refinement result ($R_p$ = 3.96% and $R_{wp}$ = 2.49%) suggests good phase purity of **HTT-Zn** (Fig. 2a). The Fourier-transform infrared (FT-IR) spectrum shows that vanishing C=O and C–H stretching signals of the thioester chain of HVaTT at 1702 and 2850–3000 cm$^{-1}$ echoes the complete alkaline hydrolysis of the protective thioester chain and coordination of $S^-$ to $Zn^{2+}$ centres.

The residual peak at 2850–3000 cm$^{-1}$ in **HTT-Zn** originates from the –$CH_2$ stretching vibration of the ethylenediamine molecule. The disappearing S–H stretching peak at 2512 cm$^{-1}$ of HTT after coordination with $Zn^{2+}$ indicates no free HTT in **HTT-Zn** (Fig. 2c). It is worth mentioning that a significant red-shift was observed from the HTT linker to **HTT-Zn** as demonstrated by the UV-vis absorption profiles (Fig. S6, ESI†).

X-ray photoelectron spectroscopy (XPS) analysis was employed to study **HTT-Zn** (Fig. S7, ESI†) to probe the chemical environment of the elements. As demonstrated in the Zn 2p spectrum (Fig. 2d), the peaks at 1045.5 and 1022.3 eV are assigned to $Zn^{II}$ $2p_{1/2}$ and $2p_{3/2}$, respectively.[13] Deconvolution of the S 2p signals generates three doublets (Fig. 2e). The doublets at 162.27 and 163.48 eV correspond to the Zn–S coordination. Also, the doublets at 163.86 and 165.12 eV can be ascribed to the S–C on HTT,[10b] while those at 166.67 to 167.97 eV indicate the presence of oxidised sulphur, probably in the form of a thiyl radical or S=O.[10a] On the other hand, thermogravimetric (TG) curves indicate **HTT-Zn** to be thermally stable up to around 200 °C in air or a $N_2$ atmosphere (Fig. S8, ESI†). $N_2$ sorption data at 77 K reveal that **HTT-Zn** adopts a type I isotherm (Fig. S9a, ESI†), with the specific surface area calculated to be 20.416 m$^2$ g$^{-1}$ by the Brunauer–Emmett–Teller (BET) equation (Fig. S9b, ESI†). The occupancy of guest ions/molecules and interpenetration can explain the extremely low surface area.

Bearing an anionic framework, **HTT-Zn** was taken as a host to absorb the cationic lethal toxic pollutant, paraquat, a widely used herbicide. Since there are few reports on the colorimetric detection of paraquat,[14] we speculate the big clear yellow **HTT-Zn** block to be a naked-eye sensor of paraquat. Specifically, a few grains of **HTT-Zn** crystals from the MeOH stock solution were taken in a Petri dish (diameter: 35 mm; depth: 10 mm). After soaking MeOH with tissue or filter paper, a few drops of paraquat diiodide (PDI) aqueous solution were added to the crystals. By microscopic or naked-eye observation, **HTT-Zn** crystals were found to darken significantly (Fig. 3a and b), and the darkening intensifies with higher PDI concentrations (Fig. S10, ESI†). The $^1$H NMR spectrum obtained from the digestion of PDI-treated **HTT-Zn** in DCl/DMSO-$d_6$ shows paraquat signals, revealing the paraquat absorption by **HTT-Zn** (Fig. S11, ESI†).

 

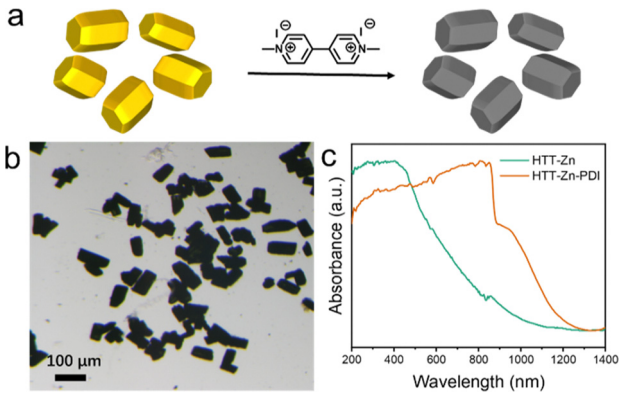


Fig. 3 (a) Schematic diagram showing PDI sensing by **HTT-Zn**; (b) optical photograph of the PDI-treated **HTT-Zn** crystals ([PDI] = 1000 ppm) under a microscope; (c) UV-vis absorption spectra of **HTT-Zn** before and after PDI treatment.

Significant red shift of optical absorption from **HTT-Zn** to PDI-treated **HTT-Zn** demonstrates the darkening of **HTT-Zn** upon exposure to PDI spectroscopically (Fig. 3c). Presumably, a strong narrow-gap donor–acceptor junction establishes between positive paraquat (acceptor) and negative electron-rich **HTT-Zn** (donor) and exhibits absorption covering the whole visible spectral region (*i.e.* dark crystals of PDI-treated **HTT-Zn**). Consistent PXRD patterns and FT-IR spectra of **HTT-Zn** before and after PDI treatment indicate the structural integrity of **HTT-Zn** throughout the sensing (Fig. S12 and S13, ESI†).

In short, utilising the masked strategy, we successfully extend the members of the thiolate-coordinated S-MOFs from heavy metals ($Pb^{II}$) to first-row transition metals ($Zn^{II}$ this time), highlighting the generality of this strategy to assemble S-MOFs. Success in preparing single crystals, resolving the structure of **HTT-Zn** and facile response to positively charged pollutants by **HTT-Zn** undoubtedly fuels up fundamental and application study of metal-thiolate-connected S-MOFs, which was once tricky because of the challenging preparation of structurally well-defined S-MOFs.

This work was supported by the National Natural Science Foundation of China (22371054, 22301045), the Foundation of Basic and Applied Basic Research of Guangdong Province (2024A1515012801), the Science and Technology Planning Project of Guangdong Province (2023A0505050164), and the Postdoctoral Fellowship Program of CPSF (GZC20240311). We also thank the Instrumental Analysis Centre of Guangdong University of Technology for collecting UV-vis absorption spectra, SEM images, and XPS measurements.

## Data availability

The data supporting this article have been included as part of the ESI.† Crystallographic data for **HTT-Zn** has been deposited at Cambridge Crystallographic Data Centre as CCDC 2407349,† accessible from **https://www.ccdc.cam.ac.uk/structures**.

## Conflicts of interest

There are no conflicts to declare.

## Notes and references

1 (*a*) X. Deng, S.-L. Zheng, Y.-H. Zhong, J. Hu, L.-H. Chung and J. He, *Coord. Chem. Rev.*, 2022, **450**, 214235; (*b*) L. Wang, A. Sarkar, G. L. Grocke, D. W. Laorenza, B. Cheng, A. Ritchhart, A. S. Filatov, S. N. Patel, L. Gagliardi and J. S. Anderson, *J. Am. Chem. Soc.*, 2023, **145**, 8486–8497.
2 (*a*) J.-M. Li, Q.-C. Lin, N. Li, Z.-H. Li, G. Tan, S.-J. Liu, L.-H. Chung, W.-M. Liao, L. Yu and J. He, *Adv. Funct. Mater.*, 2023, **33**, 2210717; (*b*) N. Li, G.-Q. Lai, L.-H. Chung, F. Yu, J. He and Y.-Q. Lan, *CCS Chem.*, 2023, **6**, 1211–1221.
3 (*a*) A. J. Clough, J. W. Yoo, M. H. Mecklenburg and S. C. Marinescu, *J. Am. Chem. Soc.*, 2015, **137**, 118–121; (*b*) Y. Liu, X. Li, S. Zhang, Z. Wang, Q. Wang, Y. He, W.-H. Huang, Q. Sun, X. Zhong, J. Hu, X. Guo, Q. Lin, Z. Li, Y. Zhu, C.-C. Chueh, C.-L. Chen, Z. Xu and Z. Zhu, *Adv. Mater.*, 2023, **35**, 2300945.
4 (*a*) M.-Q. Li, Y. Cao, L. Qin, H. Cheng, W. Yang and Z. Lu, *Nano Res.*, 2023, **17**, 2181–2185; (*b*) B. Wang, J. Li, M. Ye, Y. Zhang, Y. Tang, X. Hu, J. He and C. C. Li, *Adv. Funct. Mater.*, 2022, **32**, 2112072.
5 (*a*) J. Hu, S. Chen, Z. Liu, J.-R. Li, J.-H. Huang, Z. Jiang, W. Ou, W.-M. Liao, J. Lu and J. He, *J. Mater. Chem. A*, 2023, **11**, 10577–10583; (*b*) X.-C. Zhou, C. Liu, J. Su, Y.-F. Liu, Z. Mu, Y. Sun, Z.-M. Yang, S. Yuan, M. Ding and J.-L. Zuo, *Angew. Chem., Int. Ed.*, 2023, **62**, e202211850.
6 (*a*) Y. He, J. Dong, Z. Liu, M.-Q. Li, J. Hu, Y. Zhou, Z. Xu and J. He, *ACS Appl. Mater. Interfaces*, 2022, **14**, 1070–1076; (*b*) K.-K. Yee, N. Reimer, J. Liu, S.-Y. Cheng, S.-M. Yiu, J. Weber, N. Stock and Z. Xu, *J. Am. Chem. Soc.*, 2013, **135**, 7795–7798.
7 R. Patra, S. Mondal and D. Sarma, *Dalton Trans.*, 2023, **52**, 17623–17655.
8 (*a*) P. Chen, X. Su, C. Wang, G. Zhang, T. Zhang, G. Xu and L. Chen, *Angew. Chem., Int. Ed.*, 2023, **62**, e202306224; (*b*) J.-H. Dou, M. Q. Arguilla, Y. Luo, J. Li, W. Zhang, L. Sun, J. L. Mancuso, L. Yang, T. Chen, L. R. Parent, G. Skorupskii, N. J. Libretto, C. Sun, M. C. Yang, P. V. Dip, E. J. Brignole, J. T. Miller, J. Kong, C. H. Hendon, J. Sun and M. Dincă, *Nat. Mater.*, 2021, **20**, 222–228.
9 (*a*) Z. Liu, Y. Wu, Y.-H. Zhong, L.-H. Chung, W.-M. Liao, X. Yang and J. He, *CrystEngComm*, 2023, **25**, 347–351; (*b*) H. Zhong, Z. Jiang, J. Hu, L.-H. Chung and J. He, *Chem. Commun.*, 2024, **60**, 7578–7581.
10 (*a*) L. Mendecki, M. Ko, X. Zhang, Z. Meng and K. A. Mirica, *J. Am. Chem. Soc.*, 2017, **139**, 17229–17232; (*b*) L. Wang, A. Daru, B. Jangid, J. H. Chen, N. Jiang, S. N. Patel, L. Gagliardi and J. S. Anderson, *J. Am. Chem. Soc.*, 2024, **146**, 12063–12073.
11 (*a*) J. Hu, J.-Z. Xiao, W.-M. Liao, S. Liu, J. Li, Y. He, L. Yu, Q. Li, G. Xu and J. He, *J. Mater. Chem. A*, 2023, **11**, 11463–11470; (*b*) J. Huang, Y. He, M.-S. Yao, J. He, G. Xu, M. Zeller and Z. Xu, *J. Mater. Chem. A*, 2017, **5**, 16139–16143.
12 R. Cini, *J. Biomol. Struct. Dyn.*, 1999, **16**, 1225–1237.
13 (*a*) J. Y. Choi, M. Stodolka, N. Kim, H. T. B. Pham, B. Check and J. Park, *Chem*, 2023, **9**, 143–153; (*b*) T.-L. Pu, X.-Y. Wang, Z.-B. Sun, X.-Y. Dong, Q.-Y. Wang and S.-Q. Zang, *Angew. Chem., Int. Ed.*, 2024, **63**, e202402363; (*c*) R. Sakamoto, K. Hoshiko, Q. Liu, T. Yagi, T. Nagayama, S. Kusaka, M. Tsuchiya, Y. Kitagawa, W.-Y. Wong and H. Nishihara, *Nat. Commun.*, 2015, **6**, 6713; (*d*) Z.-L. Zheng, M.-M. Wu, X. Zeng, X.-W. Zhu, D. Luo, X.-L. Chen, Y.-F. Chen, G.-Z. Yang, D.-S. Bin, X.-P. Zhou and D. Li, *Angew. Chem., Int. Ed.*, 2024, **63**, e202400012.
14 (*a*) H. Li, D.-X. Chen, Y.-L. Sun, Y. B. Zheng, L.-L. Tan, P. S. Weiss and Y.-W. Yang, *J. Am. Chem. Soc.*, 2013, **135**, 1570–1576; (*b*) J. Gu, X. Li, Z. Zhou, R. Liao, J. Gao, Y. Tang and Q. Wang, *Chem. Eng. J.*, 2019, **368**, 157–164; (*c*) X. Li, M. Li, Y. Chen, G. Qiao, Q. Liu, Z. Zhou, W. Liu and Q. Wang, *Chem. Eng. J.*, 2021, **415**, 128975; (*d*) Z. Zhou, X. Li, Y. Tang, C. C. Zhang, H. Fu, N. Wu, L. Ma, J. Gao and Q. Wang, *Chem. Eng. J.*, 2018, **351**, 364–370.